

Article

# Comparative Efficacies of a 3D-Printed PCL/PLGA/ $\beta$ -TCP Membrane and a Titanium Membrane for Guided Bone Regeneration in Beagle Dogs

Jin-Hyung Shim <sup>1,†</sup>, Joo-Yun Won <sup>2,†</sup>, Su-Jin Sung <sup>3,†</sup>, Dong-Hyuk Lim <sup>1</sup>, Won-Soo Yun <sup>1</sup>, Young-Chan Jeon <sup>3</sup> and Jung-Bo Huh <sup>3,\*</sup>

Received: 12 August 2015 ; Accepted: 10 October 2015 ; Published: 21 October 2015

Academic Editor: Jianxun Ding

<sup>1</sup> Department of Mechanical Engineering, Korea Polytechnic University, 237 Sangdaehak-Ro, Siheung-Si, Gyeonggi-Do 15073, Korea; happyshim@kpu.ac.kr (J.-H.S.); thmim123@naver.com (D.-H.L.); wsyun@kpu.ac.kr (W.-S.Y.)

<sup>2</sup> Research Institute, T&R Biofab Co. Ltd., 237 Sangdaehak-Ro, Siheung-Si, Gyeonggi-Do 15073, Korea; jyun@tnrbiofab.com

<sup>3</sup> Department of Prosthodontics, Dental Research Institute, Biomedical Research Institute, School of Dentistry, Pusan National University, YangSan, Gyeongnam 676-870, Korea; bogus0215@naver.com (S.-J.S.); jeonyc@paran.com (Y.-C.J.)

\* Correspondence: huhjb@pusan.ac.kr; Tel.: +82-55-360-5146; Fax: +82-55-360-5134

† These authors contributed equally to this work.

**Abstract:** This study was conducted to evaluate the effects of a 3D-printed resorbable polycaprolactone/poly(lactic-co-glycolic acid)/ $\beta$ -tricalcium phosphate (PCL/PLGA/ $\beta$ -TCP) membrane on bone regeneration and osseointegration in areas surrounding implants and to compare results with those of a non-resorbable titanium mesh membrane. After preparation of PCL/PLGA/ $\beta$ -TCP membranes using extrusion-based 3D printing technology; mechanical tensile testing and *in vitro* cell proliferation testing were performed. Implant surgery and guided bone regeneration were performed randomly in three groups (a no membrane group, a titanium membrane group, and a PCL/PLGA/ $\beta$ -TCP membrane group ( $n = 8$  per group)). Histological and histometric analyses were conducted to evaluate effects on bone regeneration and osseointegration. Using the results of mechanical testing; a PCL/PLGA/ $\beta$ -TCP ratio of 2:6:2 was selected. The new bone areas (%) in buccal defects around implants were highest in the PCL/PLGA/ $\beta$ -TCP group and significantly higher than in the control group ( $p < 0.05$ ). Bone-to-implant contact ratios (%) were also significantly higher in the PCL/PLGA/ $\beta$ -TCP and titanium groups than in the control group ( $p < 0.05$ ). When the guided bone regeneration procedure was performed using the PCL/PLGA/ $\beta$ -TCP membrane; new bone formation around the implant and osseointegration were not inferior to those of the non-resorbable pre-formed titanium mesh membrane.

**Keywords:** PCL/PLGA/ $\beta$ -TCP; 3D printing; titanium membrane; guided bone regeneration; osseointegration; beagle dog

## 1. Introduction

Dental implants for replacing missing teeth in partially or completely edentulous patients have been widely recognized in the last decade as a routine treatment modality that provides reliable long-term results [1–3]. For long-term prognoses and for acceptable aesthetic and functional outcomes for implant-supported restorations, sufficient bone must be provided to recipient sites [4–6].

Nevertheless, in cases of periodontal diseases, trauma, or atrophy, ideal implant placement is restricted due to insufficient alveolar bone [3,4]. In clinical cases of limited alveolar bone defect treatment, guided bone regeneration (GBR) has been most frequently documented and is reportedly the most commonly used [5–7].

The GBR principles introduced in 1959 by Hurley *et al.* [8] involve the placement of a mechanical barrier membrane to contain blood clots and isolate bone defects from surrounding connective tissues, thus providing bone-forming cells with access to an enclosed space intended for bone regeneration [9,10]. Of the variety of different barrier membrane materials [11] that have been used for successful GBR, extended polytetrafluoroethylene (e-PTFE) [12,13] and titanium mesh [14] are widely accepted in the clinical setting as non-resorbable membranes that induce minimal immunologic reactions and have excellent space-making ability. However, they require a second surgery for membrane removal and have a high risk of premature membrane exposure [6,11]. On the other hand, resorbable collagen [15] does not require a second surgery and shows excellent hemostasis, early wound stabilization, and provides chemotaxis for fibroblasts, but its limitations include unfavorable mechanical properties, lack of space-making ability due to rapid degradation, and early loss of barrier function [11,14].

To overcome these limitations, studies on scaffold fabrication have been conducted using biodegradable synthetic polymers. The methods used include solvent casting/particulate leaching [16], phase separation [17], emulsion freeze-drying [18], gas formation [19], and fiber bonding [20]. Three-dimensional (3D) scaffolds can be easily prepared using these methods, but control of scaffold pore geometry and pore interconnectivity is difficult [21,22], and the cytotoxic organic solvents required can damage cells or tissues [21]. Thus, safe and novel methods to overcome these problems are required. 3D printing is one such method that is based on the recently developed computer-aided design (CAD)/computer-assisted manufacturing (CAM) system [23,24]. Using this method, 3D scaffolds with a controllable pore size, porosity, and fully interconnected architecture can be prepared without the use of organic solvents.

The multi-head deposition system (MHDS) [22], an extrusion-based 3D printing technology, can be used to fabricate 3D scaffolds conveniently and quickly. In a previous study by Kim *et al.* [25], various types of scaffold were fabricated using a MHDS from a combination of biodegradable polymers, such as, polycaprolactone (PCL) and poly(lactic-co-glycolic acid) (PLGA), and bio-ceramic materials, like tricalcium phosphate (TCP), and subjected to mechanical testing and cell interaction analysis. Of the 3D-printed scaffolds, blended PCL/PLGA/TCP scaffold showed the greatest compressive strengths and moduli and greatest human bone marrow stromal cells (hBMSC) adhesion and proliferation. Shim *et al.* [26] also fabricated membrane-typed scaffolds with blended PCL/PLGA and PCL/PLGA/ $\beta$ -TCP, and evaluated their abilities to promote new bone formation in rabbit calvarial defects.

In the present study, a PCL/PLGA/ $\beta$ -TCP membrane prepared using a 3D printing system was subjected to *in vitro* mechanical and cellular tests, applied *in vivo* in a clinical setting, and compared with a titanium membrane commonly used in clinics. Implants were placed in the extracted mandibles of beagle dogs, and then the GBR procedure was performed on buccal open defect sites using the PCL/PLGA/ $\beta$ -TCP and pre-formed titanium mesh-typed membranes. Histological and histometric analyses were conducted to evaluate the effects of the 3D-printed resorbable PCL/PLGA/ $\beta$ -TCP membrane on bone regeneration ability and osseointegration in areas surrounding implants and results were compared with those of a non-resorbable titanium mesh membrane.

## 2. Experimental Section

### 2.1. Preparation of PCL/PLGA/ $\beta$ -TCP Membranes Using 3D Printing Technology

#### 2.1.1. Preparation of Blended PCL/PLGA/ $\beta$ -TCP

$\beta$ -TCP (average diameter 100 nm; Berkeley Advanced Biomaterials Inc., Berkeley, CA), PCL (19561-500G, 43,000–50,000  $M_w$ ; Polysciences Inc., Warrington, PA, USA), and PLGA (430471-5G, 50,000–75,000  $M_w$ ; Sigma-Aldrich, St. Louis, MO, USA) were admixed using a thermal melting process, as previously described [27]. PLGA (0.6 g) and PCL (0.2 g) granules were melted and blended in a glass container at 130 °C for 10 min, and then  $\beta$ -TCP (0.2 g) powder was combined with the molten PCL and PLGA and mixed for 5 min. The PCL/PLGA/ $\beta$ -TCP mix was transferred to a 10 mL steel syringe attached to an extrusion-based 3D printing system and dispensed at 135 °C.

#### 2.1.2. Fabrication of Freeform-Typed PCL/PLGA/ $\beta$ -TCP Membranes Using 3D Printing Technology

The 3D printing system had four temperature, pneumatic pressure, and motion controlled printing heads [28]. Four layers were stacked to produce the 3D-printed membranes. The 3D CAD model (Figure 1a) of the PCL/PLGA/ $\beta$ -TCP membranes for *in vivo* experiments were arranged like that of the pre-formed titanium mesh membrane (Figure 1b) (SMARTbuilder™ SB2, Osstem Co., Seoul, Korea). To enable membranes to adhere to implants, a round dome-shaped hole (3 mm in diameter) was designed. PCL/PLGA/ $\beta$ -TCP membranes had overall dimensions of 14.4 mm  $\times$  9.3 mm  $\times$  0.27 mm. In order to prepare a 2D flat mesh using the 3D printing system, the CAD data of the model were transferred to in-house coding software and the mold design was adopted to fabricate a semi-dome shaped PCL/PLGA/ $\beta$ -TCP membrane.

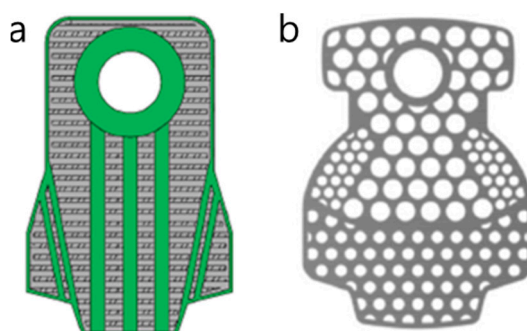


**Figure 1.** Schematic diagram of the GBR membranes used in this study. (a) 3D CAD model design of the PCL/PLGA/ $\beta$ -TCP membrane; (b) Design of pre-formed titanium mesh membrane. Guided Bone Regeneration (GBR). Computer-Aided Design (CAD). Polycaprolactone (PCL). Poly(lactic-co-glycolic acid) (PLGA). Tricalcium phosphate (TCP).

### 2.2. Mechanical Testing of PCL/PLGA/ $\beta$ -TCP Membranes

A mesh-type specimen was fabricated using the 3D printing system for mechanical tensile testing. The experimental conditions were as described by ISO527 [29], and specimen dimensions were in accord with ISO527-3 (specimen type 4). Tensile testing was performed using a single column tensile test machine (Instron Co., Model 3345, Norwood, MA, USA). Overall specimen dimensions were 42.2 mm  $\times$  10.5 mm  $\times$  0.27 mm, the printed strut size was 300  $\mu$ m, and the specimen pore size was 200  $\mu$ m. The tensile testing speed was 5 mm/min.

### 2.3. In Vitro Experiments

*In vitro* cell proliferation testing was performed to verify the effect of materials on cellular activity. Titanium and 3D-printed PLGA, PCL, PCL/PLGA, PCL/PLGA/ $\beta$ -TCP membranes were

prepared for the *in vitro* test. The dimensions and shapes of scaffolds were identical. Fibroblast cells (NIH3T3, ATCC #CRL-1658) and osteoblast cells (MG63, ATCC #CRL-1427) were cultured in Dulbecco's Modified Eagle Medium (DMEM) and DMEM Glutamax<sup>TM</sup> containing 10% FBS, 1% penicillin, and 1% streptomycin (all from Invitrogen, Carlsbad, CA, USA). Before seeding cells, all scaffolds (8 mm × 8 mm × 0.3 mm) were pre-wetted in culture medium for 2 h, irradiated with UV for 30 min, and then placed in a 24-well plate. Cells ( $3 \times 10^5$ ) were seeded on each scaffold and cultured (media were changed every other day). Cell proliferations on scaffolds were analyzed using a Cell Counting Kit-8 (CCK-8, Dojindo, Rockville, MD, USA) after incubation for at 1, 4, 7, and 14 days.

#### 2.4. Scanning Electron Microscope (SEM) Analysis

The morphology of the PCL/PLGA/ $\beta$ -TCP membrane was observed by high resolution scanning electron microscopy (HR-SEM) using an acceleration voltage of 10 kV (FEI, Nova NanoSEM 450, Hillsboro, NJ, USA). To observe cell morphologies, cultured cells on scaffolds were fixed with 2.5% glutaraldehyde, washed twice with Phosphate Buffered Saline (PBS), and dehydrated in a 30%, 50%, 70%, 90% and 100% ethanol series.

#### 2.5. In Vivo Study

##### 2.5.1. Experimental Animals

This study was performed after obtaining the approval of the Ethics Committee on Animal Experimentation of Chonnam National University (CNU IACUC-TB-2013-10). Three 3-year-old beagle dogs with weights of 13 to 15 kg were chosen for the study. After a two-week acclimatization period, animals were provided a soft food diet and allowed free access to water.

##### 2.5.2. Tooth Extraction

The first surgery was performed to extract first molars and premolars on lower jaws. After atropine sulfate induction (0.05 mg/kg Intramuscular injection (IM); Dai Han Pharm Co., Seoul, Korea), animals were anaesthetized with isoflurane (Choongwae Co., Seoul, Korea). Mucosa at the operation site was injected with 1 mL of 2% lidocaine HCL (Yu-Han Co., Gunpo, Korea) and 1:100,000 epinephrine. Targeted premolars and first molars were split into two parts, that is, into mesial and distal roots. Buccal, lingual, and lateral walls of alveolar sockets were carefully preserved. The teeth were extracted so as not to cause any damage to the extraction site, which was sutured with 4-0 nylon (Mersilk, Ethicon Co., Livingston, UK) to accelerate the healing process. Animals were allowed a two-month recovery period.

##### 2.5.3. Implant Surgery and Guided Bone Regeneration Procedures

Implant surgery and GBR were carried after the two-month recovery period. Local and general anesthesia were as described for tooth extraction. Briefly, in each animal, prior to implant insertion, the alveolar ridge was adjusted approximately by 1.5 mm to form a flat ridge, and a 2.5 mm deep buccal open defect model was made ( $n = 8$  defects per animal). This specific model did not have the buccal bone around the 2.5 mm upper thread area of the implant as shown in Figure 2. Implants (TSIII,  $\Phi 3.5$  mm × H7.0 mm, Osstem Co., Seoul, Korea) were applied ( $n = 8$  implants per animal) in edentulous mandibular alveolar ridges. The 4.5 mm implant fixture was installed inside the reduced alveolar ridge to form a 2.5 mm peri-implant buccal open defect (Figure 3a). A height connector (SMARTbuilder<sup>TM</sup> SB Anchor for TS,  $\Phi 4.0$  mm × H 0.5 mm, Osstem Co., Seoul, Korea) was used to connect membranes to each implant. Deproteinized bovine bone grafting material (Bio-Oss, Geistlich Biomaterials, Wolhusen, Switzerland) was used to fill all defects. The graft material was dampened with sterile saline for five minutes and then was placed into open buccal defects. Following grafting, a PCL/PLGA/ $\beta$ -TCP membrane or pre-formed titanium mesh membrane (SMARTbuilder<sup>TM</sup> SB2, Osstem Co., Seoul, Korea) was placed randomly on buccal open defects (Figure 3b). Membranes were

placed over entire defects and covered 2–3 mm of adjacent alveolar bone to enhance graft material stability. Bone graft material (0.125 mg) was then added to each defect. A cover screw (Cover cap, Ø4.0 mm × H1.5 mm, Osstem Co., Seoul, Korea) was used to fix the membrane. Control group animals were treated with the bone grafting material but not with a membrane. Mucoperiosteal flaps were processed properly with 4-0 nylon (Mersilk, Ethicon Co., Livingston, UK) to achieve submerged implants. All surgeries were executed by the same professionally trained operator.

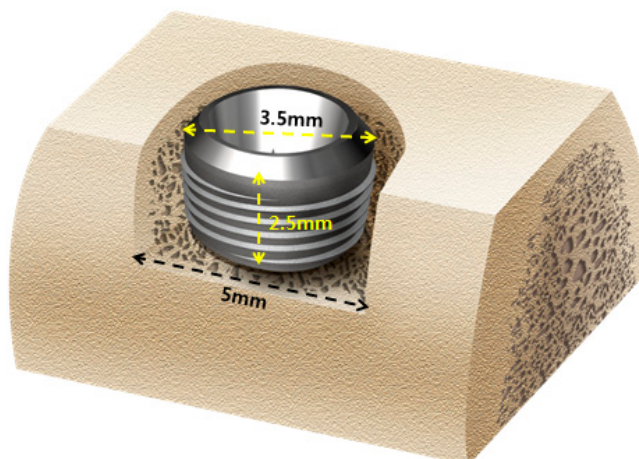


**Figure 2.** Schematic diagram of the open buccal defect model; 4.5 mm of the implant was installed inside the reduced alveolar ridge up to the reference notch, to form 2.5 mm supra-alveolar, peri-implant defects.

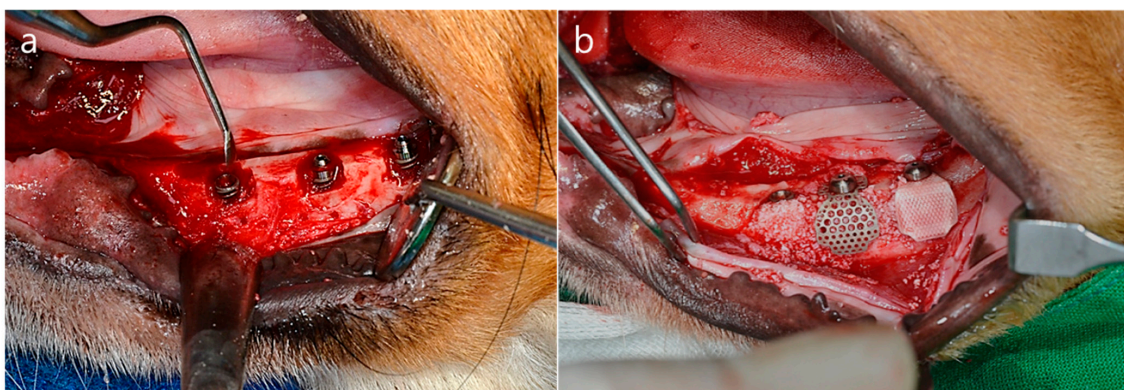


**Figure 3.** Operation procedures (a) The alveolar ridge was adjusted by approximately 1.5 mm to form a flat ridge. Buccal open defects of 2.5 mm in depth were created. Implants were placed into the edentulous mandibular alveolar ridge; (b) Bone grafting material was used to fill the defects. The membrane was added to cover the buccal open defects.

#### 2.5.4. Post-Operative Care and Sacrifice

Antibiotics, penicillin G procaine, and penicillin G benzathine (1 mL/5 kg) were administered intramuscularly immediately after surgery and again at 48 h postoperatively. Daily flushing of the oral cavity with 2% chlorhexidine gluconate was performed for plague control until study completion. Sites of interest were monitored daily to check for maintenance of suture line closure, edema, mucosal health, and evidence of tissue infection or necrosis until sutures were removed (suture materials were discarded a week after implant placement). The animals were fed a soft food diet for two weeks after surgery, followed by a regular diet, and were sacrificed at eight weeks after surgery by intravenous concentrated sodium pentobarbital injection (Euthasol, Delmarva

Laboratories Inc., Midlothian, VA, USA). Block sections, including surrounding mucosa, implants, alveolar bone, and membrane, were then obtained.

### 2.5.5. Histomorphometric Analysis

Specimens were fixed in neutral buffered formalin (Sigma Aldrich, St. Louis, MO, USA) for two weeks and then dehydrated using an ethanol series (70%, 80%, 90%, and 100%). Dehydrated specimens were embedded in Technovit 7200 resin (Heraeus KULZER, South Bend, IN, USA). Polymerized specimen blocks were sectioned longitudinally from each implant center using an EXAKT diamond cutter (KULZER EXAKT 300), and finished using an EXAKT grinding machine (EXAKT, Norderstedt, Germany) at 30  $\mu\text{m}$  from an initial 400  $\mu\text{m}$ . Specimens were stained with hematoxylin and eosin (H&E) to observe newly regenerated bone. A light microscope coupled to a computer (Olympus BX, Tokyo, Japan) and a CCD camera (Polaroid DMC2 digital microscope camera, Polaroid Corporation, Cambridge, MA, USA) was used to capture images. SPOT V4.0 software (Diagnostic Instruments Inc., Sterling Heights, MI, USA) was used to obtain all measurements.

The following parameters were examined (Figure 4):

1. New bone area percentage in opened buccal defects (NB, %)NB% was measured in the regions of bone regeneration in the spaces surrounding buccal open defects, implants, and membranes;
2. Bone-to-implant contact percentage at buccal open defects around implants (BIC, %)Bone-to-implant contact ratios were measured in regions where bone regenerated along the implant surface from the implantation lines on the alveolar ridge;
3. Intra-thread bone density in the buccal open defect area around the implant (ITBD, %)The intra-thread bone densities were measured in regions of bone regeneration along implants from implantation reference points on the alveolar ridge.

Specimen images were magnified by 12.5 $\times$ . A magnification of 100 $\times$  was chosen to accurately evaluate ITBD and BIC, and 40 $\times$  was used for the histometric analysis.

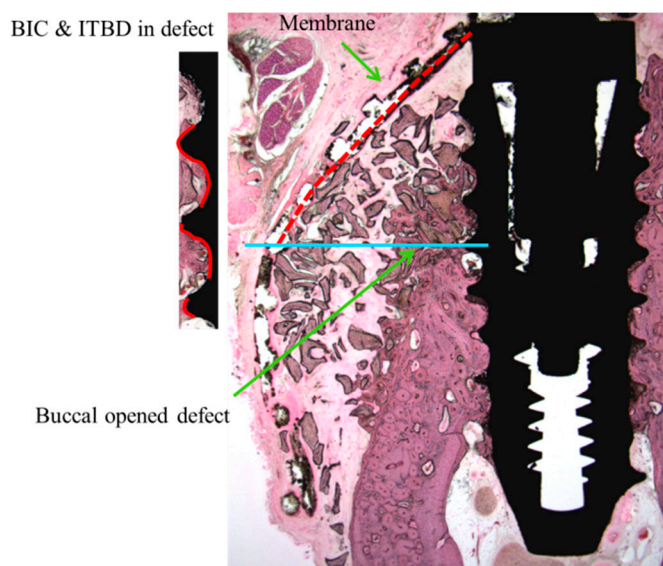


**Figure 4.** Measurements made using histologic specimens were: new bone volume in the opened buccal defect region (NB, in the space surrounding a buccal open defect, implant, and membrane, %); bone-to-implant contact ratios in the upper third thread portion of the implant in the opened buccal defect region (BIC, red line, %); and intra-thread bone density in the upper third of the threaded implant portion in the opened buccal defect region (ITBD, %). Blue line: inferior border of open buccal defect.

## 2.6. Statistical Analysis

Results are displayed as means  $\pm$  SDs. The statistical analysis was performed using SPSS ver. 21.0 (SPSS, Chicago, IL, USA). The Kruskal-Wallis test was used to analyze intergroup histometric measurement (ITBD, BIC, and NB) differences. The Mann-Whitney U test was used as a *post hoc* test ( $p < 0.05$ ). Statistical significance was accepted for  $p$  values  $< 0.05$ .

## 3. Results

### 3.1. Fabrication of PCL/PLGA/ $\beta$ -TCP Membranes Using 3D Printing Technology

Using the MHDS, GBR PCL/PLGA/ $\beta$ -TCP membranes were successfully fabricated. Figure 5 shows a PCL/PLGA/ $\beta$ -TCP membrane. The membrane included pores and a reinforced line; pore size was 250  $\mu$ m and the width of the line was 300  $\mu$ m. Membrane porosity was 40%. The printed lines were angled slanted at 60°, 120°, and 180°, and the pore structure was triangular. The thickness of the three-layered membranes was 270  $\mu$ m. Figure 6 shows SEM images of the PCL/PLGA/ $\beta$ -TCP membrane, and shows that membranes had fully interconnected, uniformly shaped pores with a rough surface.



**Figure 5.** A PCL/PLGA/ $\beta$ -TCP membrane produced using 3D printing technology. Pores were triangularly structured and completely interconnected.

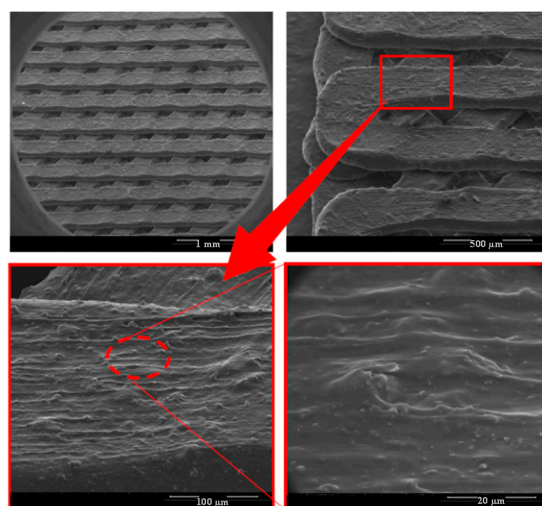


**Figure 6.** Scanning Electron Microscope (SEM) images of the prepared PCL/PLGA/ $\beta$ -TCP membrane. SEM images showed a rough surface, which was produced by incorporating TCP powder.

### 3.2. Effect of Material Blending Ratio on Mechanical Properties

To evaluate the mechanical properties of blended materials produced using different ratios, tensile testing was performed. First, the effects of PCL/PLGA ratio on mechanical properties were

examined. The elastic modulus (slope of the first linear portion of the stress-strain diagram) of the 100% PCL membrane was lower than those of blended PCL/PLGA membranes (Figure 7). The 100% PCL membrane exhibited elasticity, and the elastic modulus (indicating stiffness) increased proportionally with PLGA ratio. Blended PCL/PLGA membranes gradually became brittle as the PLGA ratio increased. In addition, tensile testing of PCL/PLGA/ $\beta$ -TCP membranes with different ratios was also conducted, as shown in Figure 8. Various ratios of PCL/PLGA/ $\beta$ -TCP were evaluated, and the ratio 2:6:2 showed the highest mechanical strength in the stress-strain plot. A GBR membrane should possess sufficient mechanical strength to provide space, and thus, a ratio of 2:6:2 was selected for the PCL/PLGA/ $\beta$ -TCP membrane used in the present study.

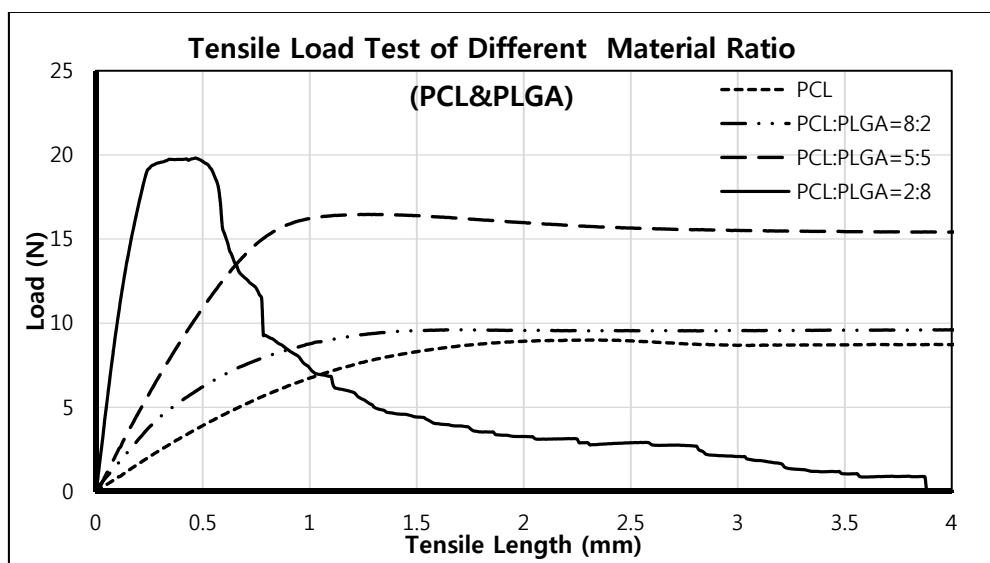


**Figure 7.** Tensile test results for different material ratios of PCL and PLGA. The elastic modulus and mechanical strength of PCL/PLGA blends gradually increased with PLGA content.

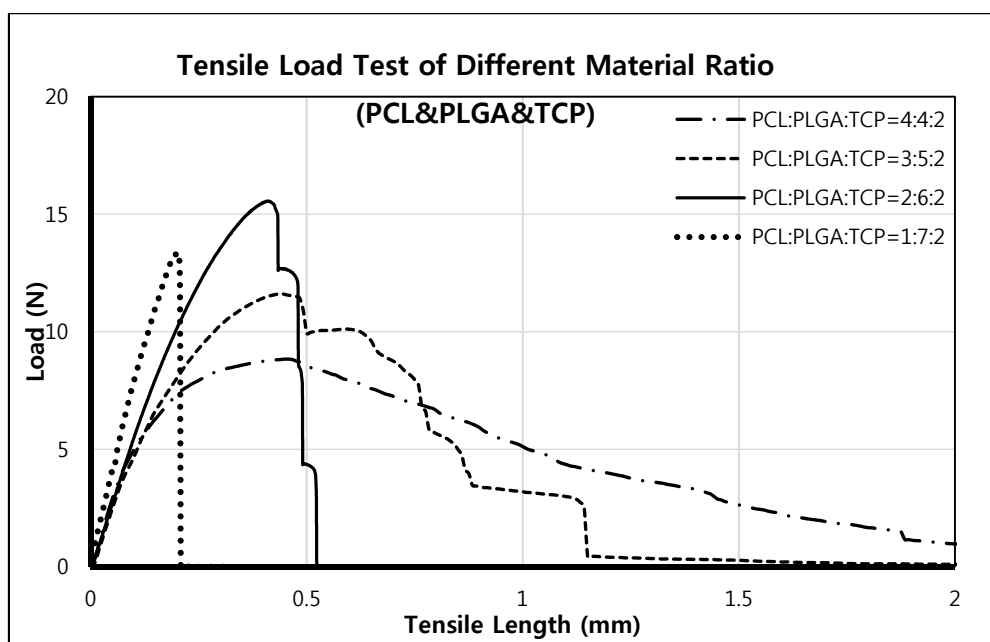


**Figure 8.** Tensile testing results of different material ratios (PCL/PLGA/ $\beta$ -TCP). A PCL/PLGA/TCP ratio of 2:6:2 showed the highest mechanical strength.

### 3.3. Effect of Material Blending Ratio on Cellular Activity

First, we seeded NIH3T3 and MG63 cells on pre-wetted scaffolds to measure cell proliferation rates. After one day, both cells were well attached on all membranes, but the optical density of PCL/PLGA/ $\beta$ -TCP (2:6:2) was greater than those of titanium, 100% PCL, and 100% PLGA. The proliferation of NIH3T3 cells on PLGA/PCL/ $\beta$ -TCP was not significantly different to that on titanium until day 7. Unexpectedly, NIH3T3 cells aggregated and detached from all bioresorbable membranes after seven days. On the other hand, the optical density of MG63 cells on PCL/PLGA/ $\beta$ -TCP was similar to that on titanium from day 7, though they were significantly different ( $p < 0.001$ ) until day 4 (Figure 9). These results suggest that the PLGA/PCL/ $\beta$ -TCP membrane could be used as a GBR membrane.

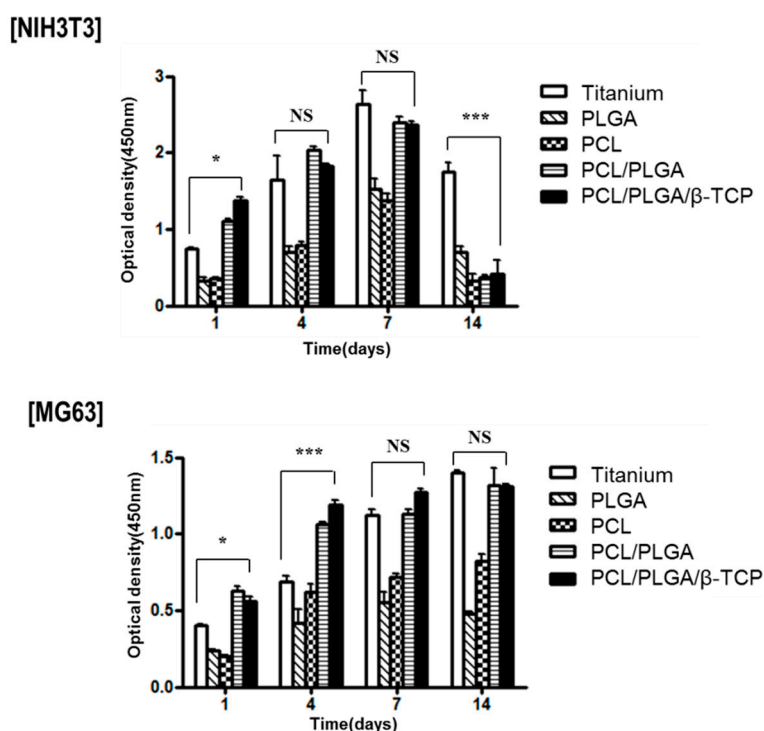


**Figure 9.** The cell proliferation assays of NIH3T3 and MG63 cells (\*  $p < 0.05$ , \*\*\*  $p < 0.001$ ; NS, no significant difference).

Next, we observed the morphologies of attached cells on membranes fixed with 2.5% glutaraldehyde. As shown Figure 10, surfaces and pores of all bioresorbable membranes were fully covered by cells on day 14, and the PLGA/PCL/ $\beta$ -TCP membrane looked flat due to confluent cells. Meanwhile, NIH3T3 cells tended to aggregate and peel off membranes on day 14, which was consistent in our *in vitro* cell proliferation assay findings.

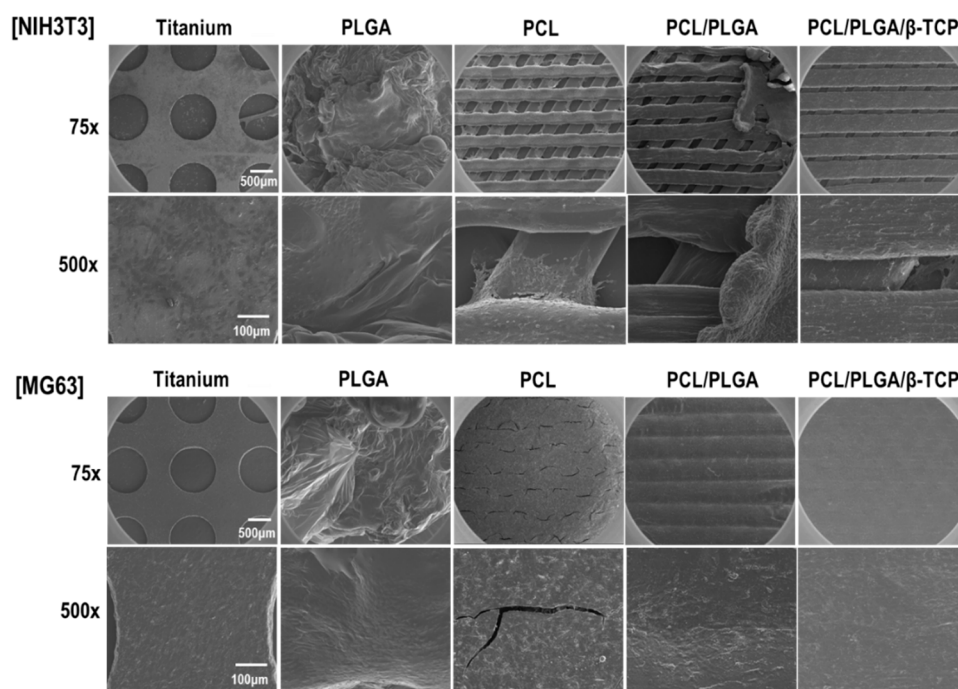


**Figure 10.** Scanning electron microscope images of NIH3T3 and MG63 cells on different bioresorbable membrane and on the non-resorbable titanium membrane.

### 3.4. In Vivo Results

#### 3.4.1. Clinical Finding

All animals successfully tolerated surgery, and all 24 implants recovered uneventfully. During the recovery period, none of the implants were exposed or lost, and no exposed or separated membrane was observed. No clinical difference was found between the three study groups.

#### 3.4.2. Histologic Findings

At eight weeks after surgery, no significant new bone formation was seen around implants in the opened buccal defect region of the control group (Figure 11); instead, a great amount of fibrous tissue was found. At the same time, due to the absence of membrane, a small amount of bone grafting material was found to be scattered in defect regions.

On the other hand, significant new bone formation was seen around implants in opened buccal defect regions in the PCL/PLGA/ $\beta$ -TCP group at eight weeks after surgery (Figure 12). Membranes were fully or partially absorbed, and remaining membranes remained structurally intact. Almost all bone graft materials were retained in defect areas, and were partially surrounded by bony tissues.

In the titanium group, significant new bone formation was observed around implants in buccal open defect regions at eight weeks (Figure 13), and membrane shapes were well maintained. Furthermore, a large amount of bone grafting material remained in defect areas, and bone graft materials were partially surrounded by bony tissues.

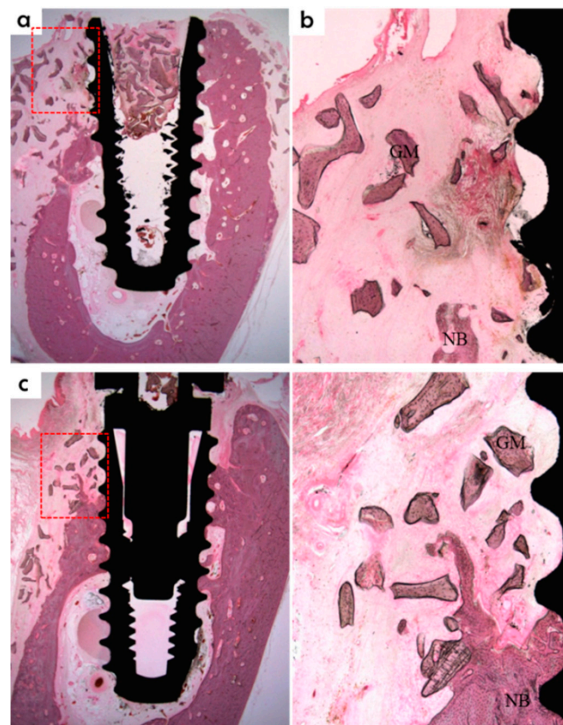


**Figure 11.** Histological sections of the control group at week 8 after operation. Little new bone was observed. GM, bone grafting material; NB, new bone. (H&E stain; original magnification 12.5 $\times$  (a) and (c); 40 $\times$  (b) and (d)). Red box in (a) is the area of (b), red box in (c) is the area of (d).

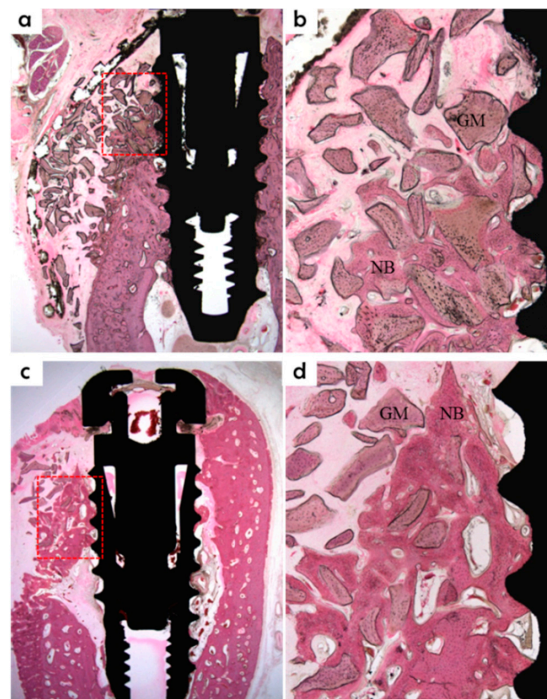


**Figure 12.** Histological sections of the PCL/PLGA/ $\beta$ -TCP group at week 8 after surgery. A significant amount of new bone formation was found. GM, bone grafting material; NB, new bone. (H&E stain; original magnification 12.5 $\times$  (a) and (c); 40 $\times$  (b) and (d)). Red box in (a) is the area of (b), red box in (c) is the area of (d).

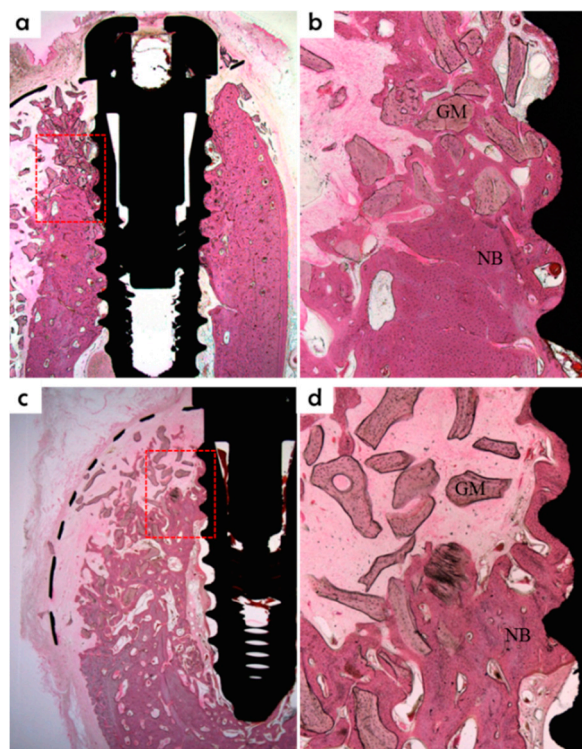


**Figure 13.** Histological sections of the titanium group at week 8 after surgery. A significant amount of new bone formation was observed. GM, bone grafting material; NB, new bone. (H&E stain; original magnification 12.5× (a) and (c); 40× (b) and (d)). Red box in (a) is the area of (b), red box in (c) is the area of (d).

### 3.4.3. Histometric Findings

Histometric measurements are summarized in Table 1. The PCL/PLGA/β-TCP group showed the highest new bone area (%) in buccal defect areas and this was significantly greater than in the control group ( $p < 0.05$ ), but not than in the titanium group ( $p > 0.05$ ). The PCL/PLGA/β-TCP and titanium groups had significantly higher bone-to-implant contact ratio (%) values than the control group. No significant difference was observed between the two experimental groups (PCL/PLGA/β-TCP and titanium) ( $p > 0.05$ ). The three groups had similar intra-thread bone densities (%) ( $p > 0.05$ ).

**Table 1.** NB (%), BIC (%), and ITBD (%) of the upper 3 threads of implants in buccal defects (means ± SDs;  $n = 8$ ).

Group	NB (%)	BIC (%)	ITBD (%)
Control	4.88 ± 3.95 <sup>a</sup>	12.31 ± 10.70 <sup>a</sup>	11.42 ± 8.51
PCL/PLGA/β-TCP	24.93 ± 5.80 <sup>b</sup>	37.53 ± 12.50 <sup>b</sup>	17.07 ± 7.12
Titanium	14.92 ± 8.63 <sup>a,b</sup>	41.90 ± 18.04 <sup>b</sup>	16.23 ± 3.98
$p^*$	0.001 <sup>*</sup>	0.003 <sup>*</sup>	0.545

NB = new bone area in buccal defects (%); BIC = bone-to-implant contact in buccal defects (%); and ITBD: intra-thread bone density in buccal defects (%). Means with the same superscript letters within a column were statistically similar by Mann-Whitney U test was used as a *post hoc* test.  $p$  values were determined using the Kruskal-Wallis test:  $* p < 0.05$ .

## 4. Discussion

Scaffolds with an inner architecture having a controllable pore geometry and a fully interconnected structure can be fabricated using 3D printing technology [30] based on

computer-aided design (CAD) and computer-assisted manufacturing (CAM) technologies using a layer-by-layer process. The 3D printing system used for this experiment had four deposition heads, a three-axis motion controller, a 650 kPa pressure controller, a 150 °C temperature controller, and CAD/CAM software. Polymer was melted using heat without using any noxious solvent and then pressure-ejected under motion control through a nozzle while controlling syringe air pressure and temperature [28]. Deposition characteristics were effectively determined by optimizing pneumatic pressure, temperature, head speed, and nozzle size. Precise 3D microstructures with architectural features smaller than 100 µm can be fabricated using this method. Moreover, a wide variety of materials can be used and rapidly fabricated using the multi-deposition head. Accordingly, precise, customized 3D scaffolds with pre-determined linear widths, pore sizes, pore geometries, and porosities can be fabricated conveniently and quickly.

The pores in GBR membranes enable the molecular transportation needed for new bone formation, and their fully interconnected inner structure enhances cell adhesion rates [31]. The optimal pore size for bone tissue engineering has been reported to be 200–400 µm [26]. Furthermore, the porous, fully interconnected structures produced integrate membranes with tissues by soft tissue penetration, which reduces the problems of membrane separation and exposure [32]. According to Lee *et al.*, pore architecture and stacking direction affect the mechanical properties of scaffolds, and the triangular type of pore has a greater compressive strength than other pore types [33]. In the present study, a GBR membrane with fully interconnected triangular pores of size 270 µm was prepared using the 3D printing system.

The PLGA used in the present study was a biodegradable synthetic polymer that is known to be effective for various tissue reconstructions due to its excellent cytocompatibility [25,34]. Nevertheless, it can only rarely be used independently to maintain scaffold shape because of its rapid degradation rate [22,32,34]. In contrast, PCL is highly elastic, which prevents early scaffold fractures [28]. However, cell affinity for PCL is lower than that for PLGA due to the high hydrophobicity of PCL [35,36]. In addition, the degradation rate of PCL is much slower than bone regeneration rates [37]. PLGA/PCL blends have biological and mechanical advantages over 100% PCL and 100% PLGA. Blended PCL/PLGA has been reported to have adequate cell affinity, a degradation rate similar to the regeneration rate of bone, and sufficient flexibility for molding when used as a GBR membrane to treat irregular bone defects [25]. In the present study, the incorporation of TCP, which has excellent biocompatibility and osteoconductivity, was used to increase compressive strength and surface area, and consequently, to enhance cell and tissue integration [32].

The crucial roles of guided bone regeneration (GBR) membranes are to prevent soft tissue invasion and to regenerate bone inside defects. Therefore, we performed *in vitro* experiments using NIH3T3 (fibroblast) and MG63 (osteoblast) cell lines, four types of bioresorbable membranes, and a non-resorbable titanium membrane. As was shown by our proliferation and SEM assays, MG63 cells attached well and proliferated on PCL/PLGA/ $\beta$ -TCP membranes, but no significant difference was observed *versus* the titanium membrane. On the other hand, fully proliferated and spreading NIH3T3 cells tended to detach from membranes from culture by day 14. This peeling-off phenomenon of NIH3T3 cells needs to be confirmed by animal testing. Based on our SEM-based morphological observations, the 100% PLGA scaffold exhibited a significant morphology due to rapid swelling in the culture medium within three days, thus, it was unable to retain the porous structure and the cell culture was discontinued.

The titanium membrane used in the present *in vivo* study was pre-formed. Therefore, no additional bending or cutting was required during surgery, and it satisfied the space-making and clinical manageability requirements of membrane design criteria [38]. The membrane was conveniently applied and could potentially shorten operative times because no additional modification was required. When a circular hole is made in the membrane, it can be directly connected to implants using a connector. According to Carpio *et al.*, membrane fixation during GBR surgery in the bone defect area around implants significantly reduced post-operative complications

and increased bone regeneration [39]. When the membrane was connected to the implant, the upper part of the membrane was fixed to prevent it from collapsing and to reduce post-operative complications, including early membrane exposure. The PCL/PLGA/ $\beta$ -TCP membrane was fabricated into a shape similar to the pre-formed titanium membrane using 3D printing technology. From the perspective of tissue engineering, the 3D printing technology can be used to produce scaffold fabrications in a repetitive manner in accordance with 3D CAD model designs.

The previous studies on GBR using the PCL/PLGA/ $\beta$ -TCP membrane have been performed on calvarial defect models in rats [28], and rabbits [26,32]. In the clinical setting, GBR is usually required to address bone defects around dental implants for bone augmentation. In the present study, implants were placed in beagle dogs to represent clinical defects, and then GBR was performed. Botticelli [40] designed the defect model used in the present study that had a buccal open defect 2.5 mm above the implant; this design was devised to examine the efficacy of a GBR membrane in terms of bone regeneration. In the present study, beagles were sacrificed at eight weeks after surgery for histomorphometric analysis, and large amounts of newly formed bone were observed in buccal bone defect areas around implants in the titanium and PCL/PLGA/ $\beta$ -TCP groups. In addition, a large amount of bone graft remained in the defect area. In the control group, the amount of newly formed bone was small, and only a negligible amount of bone graft was observed. This means the PCL/PLGA/ $\beta$ -TCP membrane wrapped up the grafts, prevented scatter, and created space for bone regeneration. At eight weeks after surgery, titanium membranes were clearly observed, whereas the PCL/PLGA/ $\beta$ -TCP membranes showed degradation. If degradation should occur faster than bone regeneration, space maintenance becomes an issue. In the clinical setting, space must be maintained for GBR for three to nine months [41]. The degradation rate of the membrane fabricated in the present study was too rapid to satisfy this condition. In the histometric analysis, the PCL/PLGA/ $\beta$ -TCP group had the greatest NB (%) value in buccal bone defect areas, and this differed significantly from the control group, but not from the titanium group. This may have been because the PCL/PLGA/ $\beta$ -TCP membrane functioned as a GBR membrane to achieve new-bone formation due to the incorporation of TCP, which is an osteoconductive material [32]. In terms of BIC (%), the PCL/PLGA/ $\beta$ -TCP and titanium groups had significantly greater values than the control group, but the difference between the two experimental groups was not significant. Furthermore, ITBD (%) values were non-significantly different between the three groups.

Unlike previous studies, a canine bone defect model was used in the present study to duplicate the clinical setting in terms of placing implants and applying GBR. We focused on the bone regeneration and osseointegration efficacies of the resorbable PCL/PLGA/ $\beta$ -TCP membrane. Although different membranes and bone defect models were not used in the present study, resorbable membranes were compared with a non-resorbable titanium mesh membrane, which is typical of the type commonly used to treatment significant, large, buccal open bone defect models in the clinical setting. In terms of new bone formation, the resorbable PCL/PLGA/ $\beta$ -TCP membrane showed almost the same degree as the titanium membrane, and was found to be effective in terms of osseointegration. The ratios of PLGA, PCL, and TCP, which are resorbable materials, determine not only membrane cell affinity and mechanical strength but also degradation rate. The PCL:PLGA:TCP weight ratio of the membrane used in the present study was 2:6:2, and, as a result, degradation developed earlier than required for GBR membranes. Further optimizing studies are required to determine an appropriate ratio.

## 5. Conclusions

In this study, we successfully fabricated a resorbable PCL/PLGA/ $\beta$ -TCP guided bone regeneration membrane with a semi-dome shape using an extrusion-based 3D printing system. When guided bone regeneration was performed in the buccal bone defect areas around implants in our canine model using the PCL/PLGA/ $\beta$ -TCP membrane, the new bone formation around

implants and osseointegration were not inferior to those of the non-resorbable, pre-formed, titanium mesh membrane.

**Acknowledgments:** This research was supported by a grant from the Korean Health Technology R&D Project through the Korean Health Industry Development Institute (KHIDI), funded by the Korean Ministry of Health & Welfare (grant number: HI14C3309). The authors thank Se Eun Kim from Chonnam National University for her contributions to the data analysis.

**Author Contributions:** Jung-Bo Huh and Jin-Hyung Shim conceived and designed the study; Jung-Bo Huh, Jin-Hyung Shim, Joo-Yun Won, Su-Jin Sung, Dong-Hyuk Lim, Young-Chan Jeon, and Jung-Bo Huh performed the experiments; Jin-Hyung Shim, Joo-Yun Won and Su-Jin Sung analyzed the data; Won-Soo Yun, Jin-Hyung Shim, Joo-Yun Won and Su-Jin Sung wrote the manuscript. All authors reviewed the final manuscript.

**Conflicts of Interest:** The authors declare no conflict of interest.

## References

1. Albrektsson, T.; Zarb, G.; Worthington, P.; Eriksson, A.R. The long-term efficacy of currently used dental implants: A review and proposed criteria of success. *Int. J. Oral Maxillofac. Implant.* **1986**, *1*, 11–25.
2. Van Steenberghe, D.; Lekholm, U.; Bolender, C.; Folmer, T.; Henry, P.; Herrmann, I.; Higuchi, K.; Laney, W.; Linden, U.; Astrand, P. Applicability of osseointegrated oral implants in the rehabilitation of partial edentulism: A prospective multicenter study on 558 fixtures. *Int. J. Oral Maxillofac. Implant.* **1990**, *5*, 272–281.
3. Chiapasco, M.; Zaniboni, M. Clinical outcomes of GBR procedures to correct peri-implant dehiscences and fenestrations: A systematic review. *Clin. Oral Implant. Res.* **2009**, *20*, 113–123. [[CrossRef](#)] [[PubMed](#)]
4. Schenk, R.K.; Buser, D.; Hardwick, W.R.; Dahlin, C. Healing pattern of bone regeneration in membrane-protected defects: A histologic study in the canine mandible. *Int. J. Oral Maxillofac. Implant.* **1994**, *9*, 13–29.
5. Poli, P.P.; Beretta, M.; Cicciù, M.; Maiorana, C. Alveolar ridge augmentation with titanium mesh. A retrospective clinical study. *Open Dent. J.* **2014**, *8*, 148–158. [[PubMed](#)]
6. Benic, G.I.; Hämmerle, C.H. Horizontal bone augmentation by means of guided bone regeneration. *Periodontol. 2000* **2014**, *66*, 13–40. [[CrossRef](#)] [[PubMed](#)]
7. Hämmerle, C.H.; Jung, R.E. Bone augmentation by means of barrier membranes. *Periodontol. 2000* **2003**, *33*, 36–53. [[CrossRef](#)] [[PubMed](#)]
8. Hurley, L.A.; Stinchfield, F.E.; Bassett, A.L.; Lyon, W.H. The role of soft tissue in osteogenesis. An experimental study of canine spine fusions. *J. Bone Joint Surg. Am.* **1959**, *41*, 1243–1254. [[PubMed](#)]
9. Dahlin, C.; Sennerby, L.; Lekholm, U.; Linde, A.; Nyman, S. Generation of new bone around titanium implants using a membrane technique: An experimental study in rabbits. *Int. J. Oral Maxillofac. Implant.* **1989**, *4*, 19–25.
10. Hempton, T.J.; Fugazzotto, P.A. Ridge augmentation utilizing guided tissue regeneration, titanium screws, freeze-dried bone, and tricalcium phosphate: Clinical report. *Implant Dent.* **1994**, *3*, 35–37. [[CrossRef](#)] [[PubMed](#)]
11. Liu, J.; Kerns, D.G. Mechanisms of guided bone regeneration: A review. *Open Dent. J.* **2014**, *8*, 56–65. [[CrossRef](#)] [[PubMed](#)]
12. Dahlin, C.; Andersson, L.; Linde, A. Bone augmentation at fenestrated implants by an osteopromotive membrane technique. A controlled clinical study. *Clin. Oral Implant. Res.* **1991**, *2*, 159–165. [[CrossRef](#)]
13. Buser, D.; Dula, K.; Belser, U.C.; Hirt, H.P.; Berthold, H. Localized ridge augmentation using guided bone regeneration. 1. Surgical procedure in the maxilla. *Int. J. Periodontics Restor. Dent.* **1993**, *13*, 29–45.
14. Rakhmatia, Y.D.; Ayukawa, Y.; Furuhashi, A.; Koyano, K. Current barrier membranes: Titanium mesh and other membranes for guided bone regeneration in dental applications. *J. Prosthodont Res.* **2013**, *57*, 3–14. [[CrossRef](#)] [[PubMed](#)]
15. Oh, T.J.; Meraw, S.T.; Lee, E.J.; Giannobile, W.V.; Wang, H.L. Comparative analysis of collagen membranes for the treatment of implant dehiscence defects. *Clin. Oral Implant. Res.* **2003**, *14*, 80–90. [[CrossRef](#)]
16. Mikos, A.G.; Thorsen, A.J.; Czerwonka, L.A.; Bao, Y.; Langer, R. Preparation and characterization of poly(L-lactic acid) foams. *Polymer* **1994**, *35*, 1068–1077. [[CrossRef](#)]

17. Shin, M.; Abukawa, H.; Troulis, M.J.; Vacanti, J.P. Development of a biodegradable scaffold with interconnected pores by heat fusion and its application to bone tissue engineering. *J. Biomed. Mater. Res. A* **2008**, *84*, 702–709. [[CrossRef](#)] [[PubMed](#)]
18. Hsu, Y.Y.; Gresser, J.D.; Trantolo, D.J.; Lyons, C.M.; Gangadharam, P.R.; Wise, D.L. Effect of polymer foam morphology and density on kinetics of *in vitro* controlled release of isoniazid from compressed foam matrices. *J. Biomed. Mater. Res.* **1997**, *35*, 107–116. [[CrossRef](#)]
19. Mooney, D.J.; Baldwin, D.F.; Suh, N.P.; Vacanti, J.P.; Langer, R. Novel approach to fabricate porous sponges of poly(D,L-lactic-co-glycolic acid) without the use of organic solvents. *Biomaterials* **1996**, *17*, 1417–1422. [[CrossRef](#)]
20. Ziabari, M.; Mottaghitalab, V.; Haghi, A.K. A new approach for optimization of electrospun nanofiber formation process. *Korean J. Chem. Eng.* **2010**, *27*, 340–354. [[CrossRef](#)]
21. Haugen, H.; Aigner, J.; Brunner, M.; Wintermantel, E. A novel processing method for injection-molded polyether-urethane scaffolds. Part 2. Cellular interactions. *J. Biomed. Mater. Res.* **2006**, *77*, 73–78. [[CrossRef](#)] [[PubMed](#)]
22. Kim, J.Y.; Park, E.K.; Kim, S.Y.; Shin, J.W.; Cho, D.W. Fabrication of a SFF-based three-dimensional scaffold using a precision deposition system in tissue engineering. *J. Micromech. Microeng.* **2008**. [[CrossRef](#)]
23. Hutmacher, D.W.; Sittinger, M.; Risbud, M.V. Scaffold-based tissue engineering: Rationale for computer-aided design and solid free-form fabrication systems. *Trends Biotechnol.* **2004**, *22*, 354–362. [[CrossRef](#)] [[PubMed](#)]
24. Lin, C.Y.; Kikuchi, N.; Hollister, S.J. A novel method for biomaterial scaffold internal architecture design to match bone elastic properties with desired porosity. *J. Biomech.* **2004**, *37*, 623–636. [[CrossRef](#)] [[PubMed](#)]
25. Kim, J.Y.; Yoon, J.J.; Park, E.K.; Kim, D.S.; Kim, S.Y.; Cho, D.W. Cell adhesion and proliferation evaluation of SFF-based biodegradable scaffolds fabricated using a multi-head deposition system. *Biofabrication* **2009**. [[CrossRef](#)] [[PubMed](#)]
26. Shim, J.H.; Moon, T.S.; Yun, M.J.; Jeon, Y.C.; Jeong, C.M.; Cho, D.W.; Huh, J.B. Stimulation of healing within rabbit calvarial defect by a PCL/PLGA scaffold blend with TCP using solid freeform fabrication technology. *J. Mater. Sci. Mater. Med.* **2012**, *23*, 2993–3002. [[CrossRef](#)] [[PubMed](#)]
27. Kim, J.Y.; Jin, G.Z.; Park, I.S.; Kim, J.N.; Chun, S.Y.; Park, E.K.; Kim, S.Y.; Yoo, J.; Kim, S.H.; Rhie, J.W.; *et al.* Evaluation of solid free-form fabrication-based scaffolds seeded with osteoblasts and human umbilical vein endothelial cells for use *in vivo* osteogenesis. *Tissue Eng. Part A* **2010**, *16*, 2229–2236. [[CrossRef](#)] [[PubMed](#)]
28. Shim, J.H.; Kim, J.Y.; Park, M.; Park, J.; Cho, D.W. Development of a hybrid scaffold with synthetic biomaterials and hydrogel using solid freeform fabrication technology. *Biofabrication* **2011**. [[CrossRef](#)] [[PubMed](#)]
29. *Plastics—Standards Atmospheres for Conditioning and Testing*; ISO 291; International Organization for Standardization (ISO): London, UK, 2008.
30. Kim, J.Y.; Cho, D.W. Blended PCL/PLGA scaffold fabrication using multi-head deposition system. *Microelectron. Eng.* **2009**, *86*, 1447–1450. [[CrossRef](#)]
31. Lundgren, A.K.; Sennerby, L.; Lundgren, D. Guided jaw-bone regeneration using an experimental rabbit model. *Int. J. Oral Maxillofac. Surg.* **1998**, *27*, 135–140. [[CrossRef](#)]
32. Shim, J.H.; Huh, J.B.; Park, J.Y.; Jeon, Y.C.; Kang, S.S.; Kim, J.Y.; Rhie, J.W.; Cho, D.W. Fabrication of blended polycaprolactone/poly(lactic-co-glycolic acid)/ $\beta$ -tricalcium phosphate thin membrane using solid freeform fabrication technology for guided bone regeneration. *Tissue Eng. Part A* **2013**, *19*, 317–328. [[CrossRef](#)] [[PubMed](#)]
33. Lee, J.S.; Cha, H.D.; Shim, J.H.; Jung, J.W.; Kim, J.Y.; Cho, D.W. Effect of pore architecture and stacking direction on mechanical properties of solid freeform fabrication-based scaffold for bone tissue engineering. *J. Biomed. Mater. Res. A* **2012**, *100*, 1846–1853. [[CrossRef](#)] [[PubMed](#)]
34. Tang, Z.G.; Callaghan, J.T.; Hurt, J.A. The physical properties and response of osteoblasts to solution cast films of PLGA doped polycaprolactone. *Biomaterials* **2005**, *26*, 6618–6624. [[CrossRef](#)] [[PubMed](#)]
35. Sung, H.J.; Meredith, C.; Johnson, C.; Galis, Z.S. The effect of scaffold degradation rate on three-dimensional cell growth and angiogenesis. *Biomaterials* **2004**, *25*, 5735–5742. [[CrossRef](#)] [[PubMed](#)]
36. Lam, C.X.F.; Teoh, S.H.; Hutmacher, D.W. Comparison of the degradation of polycaprolactone and polycaprolactone-( $\beta$ -tricalcium phosphate) scaffolds in alkaline medium. *Polym. Int.* **2007**, *56*, 718–728. [[CrossRef](#)]

37. Sun, H.; Mei, L.; Song, C.; Cui, X.; Wang, P. The *in vivo* degradation, absorption and excretion of PCL-based implant. *Biomaterials* **2006**, *27*, 1735–1740. [[CrossRef](#)] [[PubMed](#)]
38. Scantlebury, T.V. 1982–1992: A decade of technology development for guided tissue regeneration. *J. Periodontol.* **1993**, *64*, 1129–1137. [[CrossRef](#)] [[PubMed](#)]
39. Carpio, L.; Loza, J.; Lynch, S.; Genco, R. Guided bone regeneration around endosseous implants with anorganic bovine bone mineral. A randomized controlled trial comparing bioabsorbable *versus* non-absorbable barriers. *J. Periodontol.* **2000**, *71*, 1743–1749.
40. Botticelli, D.; Berglundh, T.; Lindhe, J. Resolution of bone defects of varying dimension and configuration in the marginal portion of the peri-implant bone. An experimental study in the dog. *J. Clin. Periodontol.* **2004**, *31*, 309–317. [[CrossRef](#)] [[PubMed](#)]
41. Carson-Mann, L.D.; Ibbott, C.G.; Griemann, R.B. Ridge augmentation with guided bone regeneration and GTAM case illustrations. *Probe* **1996**, *30*, 232–233.



© 2015 by the authors; licensee MDPI, Basel, Switzerland. This article is an open access article distributed under the terms and conditions of the Creative Commons by Attribution (CC-BY) license (<http://creativecommons.org/licenses/by/4.0/>).